ACS Catalysis

Research Article

pubs.acs.org/acscatalysis

Palladium Nanoparticles on Graphite Oxide: A Recyclable Catalyst for the Synthesis of Biaryl Cores

Subhankar Santra,[†] Pradip Kumar Hota,[†] Rangeet Bhattacharyya,[‡] Parthasarathi Bera,[§] Prasenjit Ghosh,[#] and Swadhin K. Mandal*[,†]

[†]Department of Chemical Sciences, Indian Institute of Science Education and Research − Kolkata, Nadia 741252, India

[‡]Department of Physical Sciences, Indian Institute of Science Education and Research − Kolkata, Nadia 741252, India

[§]Surface Engineering Division, CSIR-National Aerospace Laboratories, Bangalore 560017, India

[#]Departments of Chemistry and Physics, Indian Institute of Science Education and Research − Pune, Pune 411021, India

Supporting Information

ABSTRACT: The synthesis of life saving drug molecules in a cost-effective and environmentally benign pathway is of paramount significance. We present an environment friendly protocol to prepare core moieties of top selling drug molecules such as boscalid and telmisartan using Suzuki−Miyaura coupling conditions. In contrast to the traditional synthesis of these pharmaceutically important molecules, we have accomplished a graphite oxide (GO) supported palladium nanoparticles (PdNPs) based catalyst which quantitatively produced these core biaryl moieties of top selling drug molecules in a recyclable way. The catalytic activity remained unchanged even after 16 successive catalytic cycles without incorporating any palladium metal impurity in the pharmaceutically significant organic products. A detailed study including IR spectroscopy, solid state NMR spectroscopy, X-ray photoelectron spectroscopy, and DFT calculation was employed to understand the role of solid support on the nondecaying recycling ability of the catalyst during the Suzuki−Miyaura coupling reaction. The study indicates a strong chemical interaction of the different functionalities present in the GO, with the palladium centers which is primarily responsible for such sustained catalytic activity during the consecutive Suzuki−Miyaura coupling cycles.

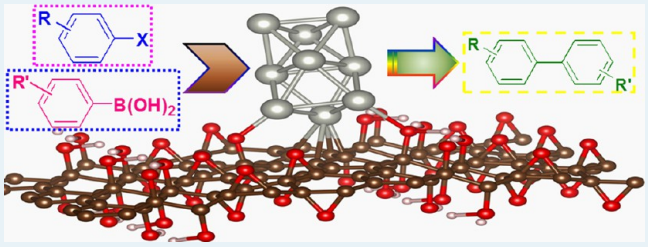

KEYWORDS: *heterogeneous catalysis, graphite oxide, palladium nanoparticles, Suzuki−Miyaura coupling, biaryls*

INTRODUCTION

The biaryl motif is a fundamental core component occurring in various biologically and pharmaceutically imperative molecules having activities like antibiotic, anti-inflammatory, antihypertensive, anticancer, antifungal, etc.[1] A trillion dollars of business per year is involved around these top selling drug molecules.[2] Figure 1 exemplifies a few top selling drug molecules, highlighting the biaryl core present in these molecules, such as antihypertensive drugs valsartan[3] and telmisartan[4] and agrochemical agent boscalid,[5] while recent researchers from GlaxoSmithKline focused on the synthesis of a selective PPARγ modulator (SPPARMγ)[6] with superior insulin sensitivity applicable for the treatment of type 2 diabetes mellitus. At present, the use of noxious phosphine based homogeneous palladium catalysts is considered as a viable route for the effective syntheses of such a biaryl core,[7] with inherent hassles like the contamination of precious metals with the product as well as the "use and throw" nature of the homogeneous catalysts.[8] The current literature does not provide any practical solution to produce these important biaryl core molecules present in top selling drugs in a recyclable way. An attractive strategy to deal with this problem could be the development of an appropriate metal nanoparticle-based heterogeneous catalyst on a solid support. Earlier, Gruttadauria and co-workers employed a palladium nanoparticles (PdNPs) based catalyst on sulfur containing ionic liquid in the synthesis of a core biaryl present in valsartan; however, the catalyst was not used in a recyclable manner.[9] It is a seemingly attractive challenge for researchers to develop an efficient and cost-effective heterogeneous catalyst based on a green support, appropriate for the quantitative synthesis of core biaryl molecules of top selling drugs in a recyclable manner. In this regard, we have picked graphite oxide (GO) as a support to anchor palladium nanoparticles (PdNPs) since it contains a variety of oxygen functionalities like epoxy, hydroxyl, carboxyl, and keto groups. These functionalities may be involved in gripping PdNPs tight on the GO surface during catalysis and ultimately providing a robust heterogeneous nanoarchitecture. The presence of a high carbon to oxygen ratio (C/O ~ 2:1) in GO[10−12] renders itself a promising green template for the decoration of palladium nanoparticles applicable in multiple catalytic transformations.[13−27] However, most of the reports comprise the synthesis of PdNPs with GO-based materials by

Received: June 20, 2013
Revised: September 9, 2013
Published: October 11, 2013

   dx.doi.org/10.1021/cs400468h | ACS Catal. 2013, 3, 2776−2789

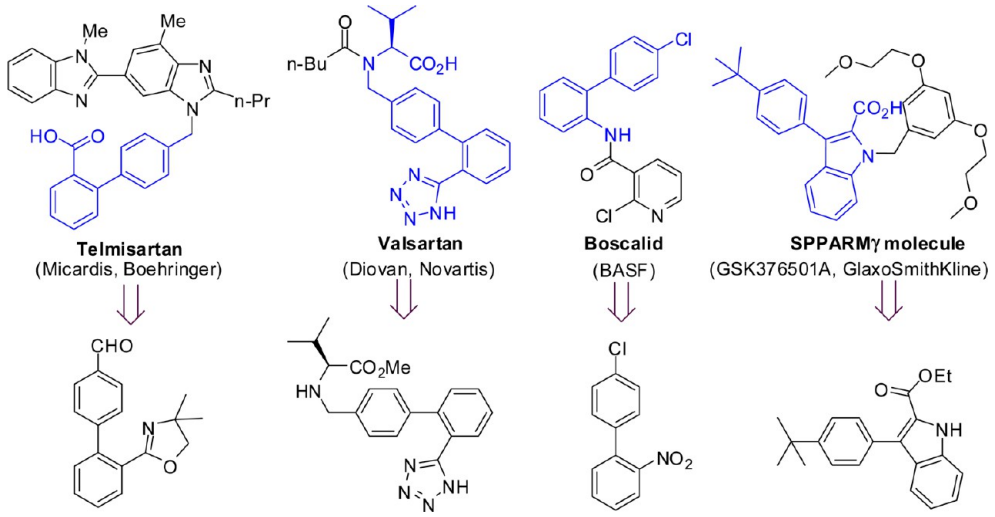

Figure 1. Examples of some top selling drug molecules containing the biaryl core. Worldwide sales: Micardis, U.S. $704 million (2004); Diovan, U.S. $3.1 billion (2004); Boscalid, € 150 million.[2] GSK376501A completed phase 1 clinical tests for the treatment of type 2 diabetes mellitus.[7]

means of either redox reaction[21] or ion exchange process[19] followed by reduction with $NaBH_4$,[20,25] molecular H_2,[15] or ethylene glycol.[22,23] Some research groups also adopted the analogous fashion for the synthesis of GO supported PdNPs in the presence of external chemical agents such as ascorbic acid,[27] surfactants,[18] or polymers.[24] Furthermore, recent approaches include a microwave assisted methodology[26] as well as the self-assembly of GO in the presence of metal salts to fabricate PdNPs over graphene-based materials.[13] It is interesting to note that most of these nanoarchitectures have been employed in electrocatalysis,[21] various gas detection studies,[23,24] hydrogenation,[18,22] oxidation,[27] and reduction[19,20] reactions, while some reports depicted the utilization of such composites in cross-coupling protocols such as Heck,[13,25] Ullmann,[14] and Suzuki–Miyaura coupling reactions.[15−17,26] El-Shall and co-workers have reported the microwave-assisted synthesis of recyclable palladium nanoparticles supported on graphene for Suzuki–Miyaura and Heck coupling reactions up to the eighth catalytic cycle with a straight substrate combination such as bromobenzene and phenyl boronic acid.[26] However, a potential recyclable heterogeneous catalyst is still missing in terms of cross-coupling reactions supported by graphitic materials which will withstand recyclability even in the presence of chemically active functional groups bearing coupling partners. From this perspective, the lack of reusable catalyst in challenging substrates bearing different active functional groups prompted us in the present study to design and synthesize PdNPs decorated on GO via thermal decomposition of palladium acetate, avoiding the use of any chemical reductant as well as any supplementary stabilizing agents such as polymers or surfactants.

Herein, we develop a GO supported palladium nanocatalyst (GO-PdNPs) by the pyrolysis of palladium acetate. The GO-PdNPs displayed diverse functional group tolerance during the Suzuki–Miyaura coupling protocol. This study for the first time established that the synthesis of biaryl core moieties of two top selling drug molecules such as boscalid and telmisartan could be accomplished without compromising its catalytic activity over a large number of successive catalytic cycles. The catalyst remained equally active until 16 consecutive catalytic cycles in the case of the boscalid nucleus without losing any efficiency, and it does not incorporate any detectable metal impurity in the organic solvent soluble part of the catalytic reaction mixture as confirmed by ICP-AES measurement. A combined approach with the aid of solid state NMR, IR, X-ray photoelectron spectroscopy, and theoretical calculation was adopted to delineate the source of the observed sustained catalytic activity of the present material.

EXPERIMENTAL SECTION

General Information. Graphite (powder <20 μm, synthetic; product order no. 282863) and palladium acetate were purchased from Sigma-Aldrich. All aryl halides, boronic acids, and other materials required for the present work were used directly as received from Sigma-Aldrich. The solvents (GR grade) were purchased from Merck, India, and were dried following standard protocols under a nitrogen atmosphere. Hexane and ethyl alcohol were purchased from Merck, India and distilled before the work-up process. The 0.22 μm PTFE membrane filter was purchased from Millipore.

^{1}H NMR and ^{13}C NMR spectra were recorded on a JEOL ECS 400 MHz spectrometer and on a Bruker Avance III 500 MHz spectrometer. Chemical shifts (δ) downfield from the reference standard were assigned positive values. Powder X-ray diffraction (PXRD) data were collected on a Rigaku Smart Lab diffractometer. Mass spectra were recorded on a Waters micromass Q-Tof micro. TEM analyses were performed either on a JEOL JEM 2011 or on a FEI TECNAI G^2 20 S-TWIN operated at 200 kV. EDX spectra were recorded on Oxford Instruments, U.K. UV–vis–NIR spectral studies were carried out on a HITACHI UV4100 spectrophotometer. AFM studies were carried out on an NTMDT instrument, model no. AP-0100, in semicontact mode after placing a 5 μL drop of dispersed solution in EtOH containing GO-PdNPs on a cleaned glass coverslip slide and allowing it to dry in the air. Raman spectroscopy was performed using the 2.54 eV (488 nm) line of an Ar ion laser on a HORIBA JOBIN YVON LabRAM HR 800 instrument by placing a pinch of the solid samples on a cleaned glass slide. The samples were platinum coated and observed through a FESEM instrument (JEOL, JSM 6700F) operating at 5 kV. ICP-AES data were recorded on a Perkin Elmer Optima 2100DV after dissolving the samples in a HCl-HNO_3 mixture. All products were isolated by short chromatography on a silica gel (100–200 mesh) column using the required ratio of hexane and ethyl acetate. The known compounds were characterized by comparing their ^{1}H and ^{13}C NMR spectra to the reported data,

dx.doi.org/10.1021/cs400468h | ACS Catal. 2013, 3, 2776−2789

and the relevant spectra are presented in the Supporting Information.

Solid State NMR Study. The solid state ^{13}C NMR spectra have been recorded on a Bruker Avance III 500 MHz spectrometer under magic angle spinning (MAS). The functional GOs are electrical conductors and hence pose severe restriction on magic angle spinning due to eddy currents. To circumvent this problem, the samples had been diluted using KBr. The gravimetric ratio of KBr and the graphene-based samples had been kept at 4:1. The spectra were collected at the MAS speed of 8000 Hz with an error of (±)1 Hz. The spectra were recorded without decoupling the proton, because (i) the MAS removes majority of the coupling and (ii) the amount of protons in the functional groups is minor.

XPS Study. XPS of GO and GO-PdNPs samples were recorded with a Thermo Fisher Scientific Multilab 2000 spectrometer using nonmonochromatic AlKα radiation (1486.6 eV) run at 15 kV and 10 mA as an X-ray source. The binding energies reported here were calculated with reference to the C 1s peak at 284.5 eV with a precision of ±0.1 eV. For XPS analysis, powder samples were mounted on the sample holder, and they were kept in the preparation chamber at UHV (10^{-9} Torr) for 5 h in order to desorb any volatile species present on the surface. After 5 h, samples were placed into an ultrahigh vacuum (UHV) chamber at 10^{-9} Torr housing the analyzer. All the spectra were obtained here in digital mode on a personal computer with 30 eV pass energy across the hemispheres of the electron analyzer and a 0.05 eV step increment. The experimental data were curve fitted into several components with Lorentzian−Gaussian peaks using the Shirley background subtraction in the Avantage software program.

Computational Details. The calculations have been performed using the Quantum-ESPRESSO (QE) software,[28] which is an implementation of the plane wave based density functional theory. Spin polarized versions of the Kohn−Sham equations are solved using ultrasoft pseudopotentials.[29] We have used a kinetic energy cutoff of 30 and 300 Ry for wave functions and charge density, respectively. The electron−electron exchange and correlation are described using Perdew, Burke, and Ernzerhof parametrization based generalized gradient approximation (GGA-PBE).[30] Brillouin zone integrations have been done with a $(9 \times 18 \times 1)$ Monkhorst−Pack k-point mesh for the (1×1) GO unit cell.[31] To speed up the convergence, we have used Marzari−Vanderbilt smearing[32] with a smearing width of 0.001 Ry. We have used a vacuum of about 11 Å in the direction normal to GO to minimize the interaction between the periodic images. The Pd nanoparticle has been modeled with a nine atom cluster. The cluster geometry considered in this calculation is the one lowest in energy as reported by Zanti and Peeters.[33] In order to study the interactions between GO and the Pd cluster, we have considered a (2×3) GO unit cell such that the distance between the Pd_9 and its periodic image is greater than 8.5 Å along all the directions.

GO does not form a nicely ordered periodic structure. On the basis of the experimental results that the C/O ratio in the samples is 2:1 and previous calculations done by Yan and Chou,[34] we choose a periodic structure in which there are strips of epoxide and hydroxyl combinations with clean graphene ribbons in between, as shown in Figure 10A. Since the −COOH and −C═O groups are typically found at the edge of the GO sheet and in our calculations we do not have edges (because of the use of periodic boundary condition), our model GO does not have the −COOH and −C═O groups.

Determining the lowest energy binding configuration of the Pd cluster on GO is quite challenging because of the several possible local minima in the potential energy surface. Since in this work we are interested in using a prototype system to understand the interactions between Pd and GO which are responsible for the stabilization of the Pd cluster on GO, we considered a few possible starting configurations, optimized their geometries by relaxing all the atoms in the unit cell, and chose the one which is lowest in energy for further analysis. The different low energy configurations of Pd_9 on GO are shown in Figure S8 (Supporting Information). We note that in order to determine the minima of the potential energy surface, one should use simulated annealing techniques,[35,36] which increases the probability of finding the global minima.

The ^{13}C NMR spectra have been calculated using the GIPAW method as implemented in QE.[37] *Ab initio* computed isotrotpic chemical shieldings, $\sigma_{iso} = Tr[\vec{\sigma}/3]$ are compared to the experimental isotropic chemical shifts by using the standard expression $\delta_{iso} = \sigma_{ref} - \sigma_{iso}$. In this work, we take σ_{ref} as 169.15 ppm such that the first peak in the computed NMR spectra of graphite corresponding to the C−O−C is aligned with respect to the peak of the experimental spectra at 59.65 ppm.

Synthesis of Graphite Oxide. Graphite oxide was synthesized using a modified Hummer's method.[38,39] A solution of 5 g of graphite (Sigma-Aldrich), 100 mL of concentrated sulfuric acid (H_2SO_4 98%), and 2.5 g of sodium nitrate ($NaNO_3$) was prepared. A total of 20 g of potassium permanganate ($KMnO_4$) was then slowly added to the solution, while keeping the mixture in an ice bath to maintain a temperature of 35 °C. The solution was continuously stirred using a standard magnetic stirrer. After an hour, the solution became quite viscous and could not be stirred any longer. The solution was held in an ice bath until it reached 10 °C. The solution was then transferred into a bigger container and was diluted with 1L deionized (DI) water. The solution was dark brown at this point. Hydrogen peroxide (H_2O_2 30%) was then slowly added until the solution turned green. To aid filtration, 50 mL of concentrated hydrochloric acid (HCl 37.5%) was added to the mixture, and the whole solution was stirred for 30 min. Graphite oxide was recovered from the solution after a four-step-wash procedure (i) washing in deionized water, centrifugation followed by filtration; (ii) washing in ethanol/HCl solution, centrifugation followed by filtration; (iii) washing in diethyl ether, centrifugation followed by filtration; and (iv) washing in diethyl ether followed by filtration. Graphite oxide was air-dried.

Synthesis of GO-PdNPs. A total of 600 mg of as-prepared graphite oxide was mixed with 300 mg of palladium acetate in a 500 mL Schlenk flask. The mixture was then kept under a vacuum for 1 h. Then under a N_2 atmosphere, 300 mL of dry toluene was added, and it was sonicated at room temperature for 1 h. During this period, exfoliation of graphite oxide occurs, followed by the arrest of palladium acetate molecules along the graphite oxide sheet. Then, the mixture was subjected to heating at 100 °C under a N_2 atmosphere for 4 h. It was cooled to room temperature (25 °C), filtered through 0.22 μm membrane filter paper, and washed sufficiently with ethanol, acetone, and finally diethyl ether. The resultant black residue was dried under a vacuum prior to use.

Synthesis of Ethyl 3-iodo-1H-indole-2-carboxylate. A solution of ethyl 1*H*-indole-2-carboxylate (2.019 g, 10.7 mmol) in dry dichloromethane (150 mL) was first cooled to 0 °C, and then recrystallized N-iodosuccinimide (NIS; 2.4074 g, 10.7 mmol) in dry dichloromethane was added in 10 min at 0 °C. The

dx.doi.org/10.1021/cs400468h | ACS Catal. 2013, 3, 2776−2789

reaction mixture was then stirred at that temperature for 12 h and left to stir at room temperature for another 12 h under a N_2 atmosphere. The reaction mixture was washed with four 50 mL portions of saturated solution of sodium carbonate followed by 50 mL of distilled water. The combined organic layers were dried over anhydrous sodium sulfate and concentrated under reduced pressure. The resultant mass was finally purified through short column chromatography (silica gel 100−200 mesh) to obtain ethyl 3-iodo-1*H*-indole-2-carboxylate as faint yellowish solid crystals (yield = 86%, see Supporting Information for details).

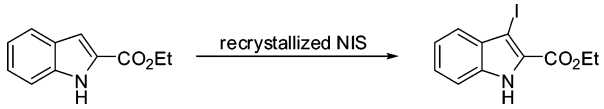

Synthesis of 2-(2-iodophenyl)-4,4-dimethyl-4,5-dihydrooxazole.[40] *Step I.* In a 1 L round-bottom flask, 2-amino-2-methyl-propanol (0.76 mL, 7.9 mmol, 1.1 equiv) and aqueous $NaHCO_3$ solution (0.5 M, 220 mL) were added to 1,4-dioxane (180 mL). 2-Iodobenzoyl chloride (2.01 g, 7.5 mmol) dissolved in 1,4-dioxane (20 mL) was added dropwise to the white suspension using a syringe for 10 min. The reaction was stirred for 3 h. Then, it was extracted with ethyl acetate and the combined organic phases were washed with HCl solution (4 M, 100 mL), NaOH solution (10 M, 100 mL), and brine solution (100 mL) respectively. Then the whole organic phase was dried over Na_2SO_4, and after removal of the solvent, the product was isolated as a white microcrystalline solid.

Step II. The resultant amide (10.20 g, 32 mmol) and 4-dimethylamino pyridine (587 mg, 4.8 mmol, 0.15 equiv) were dissolved in dry CH_2Cl_2 (200 mL), and to it, dry Et_3N (20 mL, 154 mmol, 4.8 equiv) was added. The white suspension was cooled to 0 °C, and 4-toluenesulfonyl chloride (7.41 g, 38.8 mmol, 1.2 equiv) was added. After complete addition, the suspension was allowed to warm to room temperature and stirred for 16 h. Distilled water (100 mL) was then added, and the resulting mixture was heated to reflux for 1 h. The mixture was extracted with CH_2Cl_2; the combined organic phases were washed with water and brine solution and dried over Na_2SO_4. The solvent was removed under reduced pressure, and the resultant residue was purified through short column chromatography (silica gel 100−200 mesh). The final oxazoline product was obtained as a faint green oil (yield = 59%, see Supporting Information for details).

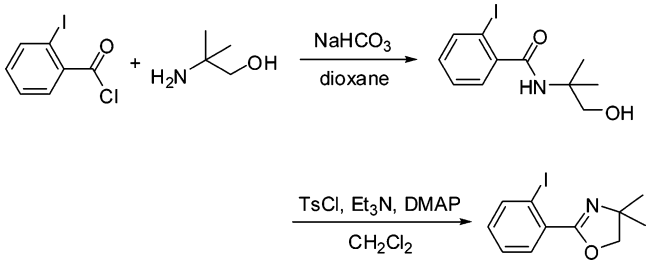

Catalytic Reaction under Dioxane-NaOMe Combination. In a 50 mL Schlenk flask, catalyst (10 mg) and solid substrates such as aryl halide (1 mmol), phenylboronic acid (1.5 mmol), and NaOMe (2 mmol) were added and kept under a high vacuum for at least 1 h. Then dry dioxane (5 mL) was added to the mixture under a N_2 atmosphere followed by the addition of liquid substrates (if any) in the requisite amounts. After that, the reaction mixture was heated at 100 °C for 24 h under a N_2 atmosphere. After completion, the reaction mixture was cooled to room temperature and evaporated under reduced pressure. The resultant mass was then purified through short column chromatography (silica gel 100−200 mesh) to obtain the final biaryl molecule (see Supporting Information for details).

Catalytic Reaction under ^{i}PrOH-K_2CO_3 Combination. In a 50 mL round bottomed flask, catalyst (10 mg), aryl halide (1 mmol), boronic acid (1.5 mmol), K_2CO_3 (2 mmol), and isopropanol (5 mL) were added and refluxed (90 °C) for 24 h. After completion, the reaction mixture was cooled to room temperature and evaporated under reduced pressure. The resultant mass was then purified through short column chromatography (silica gel 100−200 mesh) to obtain the final biaryl molecule (see Supporting Information for details).

General Procedure for Recyclability Experiments. After completion of each catalytic cycle, the reaction mixture was first cooled down to room temperature and then filtered through a 0.22 μm membrane filter, washed sufficiently with ethanol and acetone, and finally with diethyl ether. The next catalytic cycle was further carried out using the dried black residue collected on the membrane filter. The recycling experiments were performed maintaining the catalyst to substrate ratio.

One-Pot Two-Step Synthesis of Boscalid. In a 50 mL Schlenk flask, catalyst (10 mg), 2-iodoaniline (1 mmol), 4-chlorophenylboronic acid (1.5 mmol), and NaOMe (2 mmol) were added and kept under a high vacuum for at least 1 h. Then, dry dioxane (5 mL) was added to the mixture and was heated at 100 °C for 24 h under a N_2 atmosphere. After completion, the reaction mixture was cooled to room temperature, and then 2-chloronicotinoyl chloride (2 mmol) and pyridine (4 mmol) were added under a N_2 atmosphere. The reaction mixture was then heated at 100 °C for 12 h under a N_2 atmosphere, cooled to room temperature, and concentrated under reduced pressure. Boscalid was obtained as an off-white solid after short column chromatography (silica gel 100−200 mesh, see Supporting Information for details).

RESULTS AND DISCUSSION

The synthetic strategy of the catalytic material (GO-PdNPs) exploited the pyrolysis of $Pd(OAc)_2$ in the presence of GO in toluene,[41,42] avoiding the use of any reducing agent in the synthetic pathway. The generation of metallic nanoparticles through the thermolytic pathway has been explained in earlier literature which considers that the acetate ligand (OAc^-) contributes to the reduction of Pd^{2+} to Pd^0 under thermolytic conditions.[43] Microscopic techniques such as atomic force microscopy (AFM) [Supporting Information, Figure S1], scanning electron microscopy (SEM) [Supporting Information, Figure S4], and transmission electron microscopy (TEM) displayed the spherical shaped metallic nanoparticles distributed uniformly over the GO sheet (Figure 2). The TEM images unveiled a highly monodispersed nature of the palladium nanoparticles (avg. diameter = 13−14 nm), irrespective of the solvents (Figure 2A,B). The energy dispersive X-ray spectrum (EDX) collected from TEM data authenticated the presence of palladium in the GO-PdNPs (Supporting Information, Figure S3) sample.

Powder X-ray diffraction (PXRD) patterns focus light on the structural divergence of the materials; for example, the characteristic (002) peak of graphite, observable at 26.5° (2θ), has been relocated at 10.04° (2θ) in the case of graphite oxide (Figure 3). In addition to the shift of the (002) peak position, the increment in the interlayer separation value from graphite to graphite oxide (from 3.36 to 8.8 Å) reflects the inclusion of

dx.doi.org/10.1021/cs400468h | ACS Catal. 2013, 3, 2776−2789

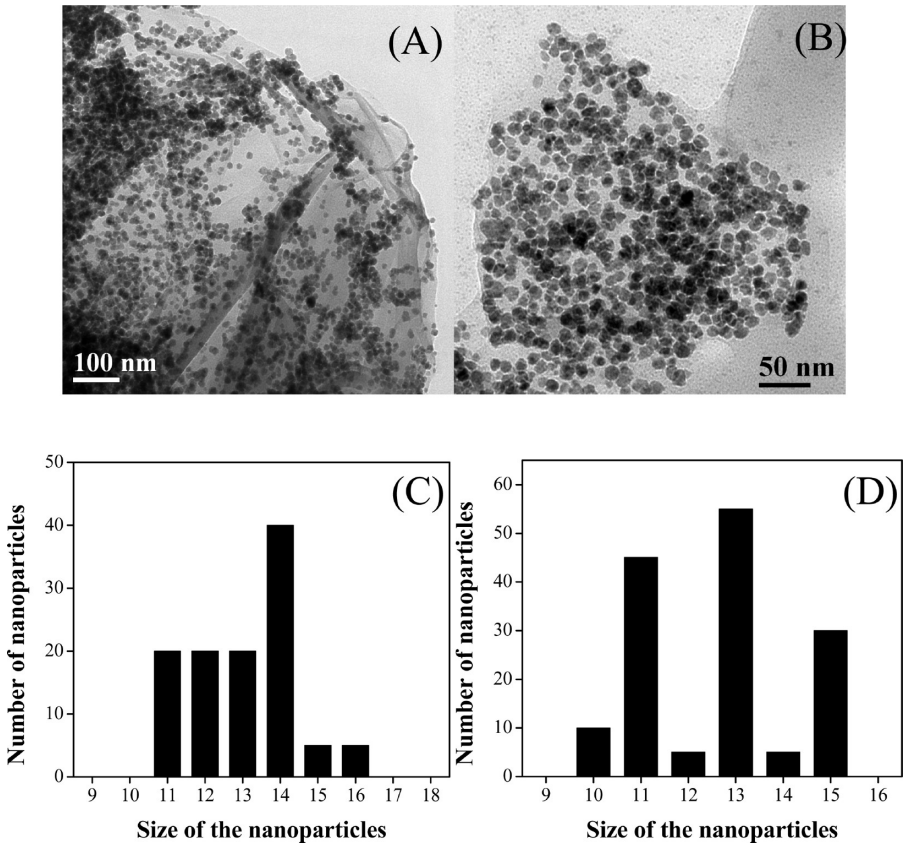

Figure 2. TEM images of GO-PdNPs from (A) ethanolic and (B) DMF-dispersions. Respective size distribution histograms from TEM images of (C) ethanolic and (D) DMF dispersions.

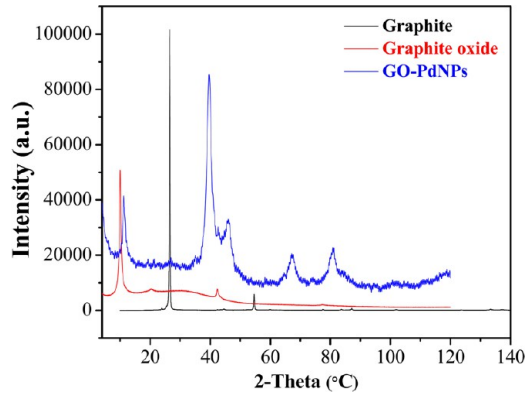

Figure 3. Powder X-ray diffraction patterns of graphite (black colored line), graphite oxide (red colored line), and GO-PdNPs (blue colored line).

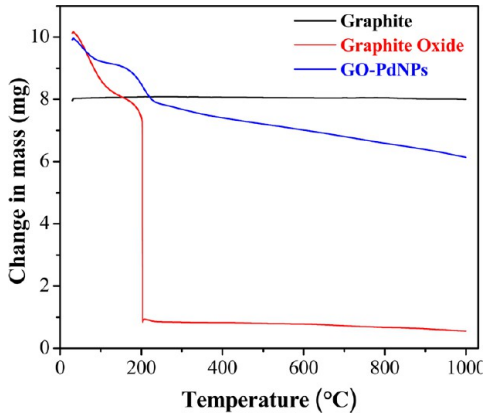

Figure 4. Thermo-gravimetric analysis graphs of graphite (black colored line), graphite oxide (red colored line), and GO-PdNPs (blue colored line).

various oxygen containing functional groups in between the layers during the oxidation process.[44] The PXRD pattern of GO-PdNPs exhibits well-defined peaks at 39.7°, 46.5°, 67.2°, and 80.9°, which can be attributed to the distinctive (111), (200), (220), and (311) crystalline planes for a face centered cubic palladium (0) lattice, respectively.[45] The preservation of the (002) peak at 10° for GO-PdNPs validates the restoration of the well-ordered lamellar structure of the GO sample in GO-PdNPs also. The structural difference has been captured in the TGA analysis of graphite, GO, and GO-PdNPs samples (Figure 4). Graphite oxide displays the weight loss in two successive steps. The first one is a steady weight loss (up to 30%, attributed to the vaporization of intercalated water molecules) which is noticed around 100 °C followed by a rapid loss (~65%, pointed toward the decomposition of functional groups) around 205 °C (red colored line) in comparison with nearly 0% weight loss of the parent graphite material in the experimental temperature range.[12,46] In contrast, GO-PdNPs has shown overall 38% weight loss in the respective temperature range. UV−vis−NIR spectroscopy of GO-PdNPs also differs from its parent material (Supporting Information, Figure S5). A similar pattern of intensity reduction in the NIR region was also observed when PdNPs were anchored onto carboxylic acid functionalized single walled carbon nanotubes.[42]

dx.doi.org/10.1021/cs400468h | ACS Catal. 2013, 3, 2776−2789

Table 1. Screening of Conditions for Suzuki−Miyaura Coupling Reaction Catalyzed by GO-PdNPs[a]

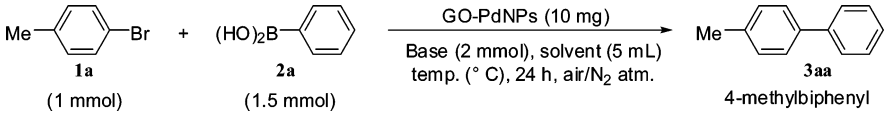

entry	solvent	base	condition	temp. (°C)	yield (%)[b]
1	DMF	Cs_2CO_3	N_2	100	48
2	dioxane	Cs_2CO_3	N_2	100	32
3	**dioxane**	**NaOMe**	**N_2**	**100**	**99**
4	toluene	NaOMe	N_2	110	85
5	THF	NaOMe	N_2	70	9
6	**^{i}PrOH**	**K_2CO_3**	**air**	**85**	**95**
7	EtOH	K_2CO_3	air	80	73
8	AcCN	K_2CO_3	air	85	58
9	water	K_2CO_3	air	100	61
10	NMP		N_2	110	–

[a]Reaction conditions: 4-Bromotoluene (1 mmol) was allowed to react with phenylboronic acid (1.5 mmol) in the presence of a base (2 mmol) employing 10 mg of the catalyst, GO-PdNPs. [b]Yields were calculated after isolation of the pure 4-methylbiphenyl through short column chromatography using silica gel (100−200 mesh).

We have chosen the Suzuki−Miyaura coupling reaction as a model one to check the feasibility of GO-PdNPs as a heterogeneous catalyst. Preliminary investigations suggest that GO-PdNPs catalyst works at its best for the coupling reaction of 4-bromotoluene with phenylboronic acid under dioxane-NaOMe and ^{i}PrOH-K_2CO_3 combinations (entries 3 and 6, Table 1). Table 1 summarizes the screening of the best reaction conditions to get the quantitative yield of 4-methylbiphenyl (**3aa**). To expand the scope of the present heterogeneous catalyst (GO-PdNPs), the Suzuki−Miyaura coupling reaction has been extended to the copious aryl halides consisting of diverse functional groups. Table 2 summarizes the catalytic activity of GO-PdNPs under the dioxane-NaOMe recipe for this particular cross-coupling reaction. After quantitative yield of 4-methylbiphenyl, bromobenzenes having electron withdrawing as well as electron donating substituents at the *para* position have been tested for this cross-coupling reaction with phenylboronic acid (**2a**). To our delight, GO-PdNPs exhibited excellent catalytic activity for aryl bromides containing nitro (−NO_2), acetyl (−C(O)Me), hydroxyl (−OH), and amine (−NH_2) functional groups (entries 1−4, Table 2) delivering respective biaryl products nearly in quantitative yield (92 to 98%). Biphenyl-4-carbaldehyde was obtained in 31% yield when 4-bromobenzaldehyde (**1f**) was coupled with phenylboronic acid (entry 5, Table 2). The functional group tolerance of the GO-PdNPs catalyst was further scrutinized when an aromatic nitrile (4-bromobenzonitrile, **1g**) and an ester (methyl 2-iodobenzoate, **1h**) were allowed to react with phenylboronic acid (**2a**) yielding biphenyl-4-carbonitrile (**3ga**) and methyl biphenyl-2-carboxylate (**3ha**) quantitatively (entries 6−7, Table 2). Successful results with phenylboronic acid have prompted us to check the feasibility of the catalyst with substituted arylboronic acids. First, 4-bromotoluene (**1a**) was reacted with substituted arylboronic acids consisting of acetyl (−C(O)Me), chloro (−Cl), methoxy (−OMe), and trifluoromethyl (−CF_3) functional groups at the *para* position of phenylboronic acid. 4-Acetylphenylboronic acid (**2b**) and 4-methoxyphenylboronic acid (**2d**) provided the coupled products at around 40% yields (entries 8 and 10, Table 2), while the trifluoromethyl phenylboronic acid (**2e**) resulted in the coupled product (**3ae**) at 71% yield (entry 11, Table 2). 4-Chloro-4′-methylbiphenyl (entry 9, Table 2) was obtained in 78% yield when 4-bromotoluene (**1a**) was allowed to couple with 4-chlorophenylboronic acid (**2c**). An unsymmetrical biaryl, 4′-methoxybiphenyl-4-carbonitrile (**3gd**), has been isolated in 85% yield upon reaction between 4-bromobenzonitrile (**1g**) and 4-methoxyphenylboronic acid (**2d**, entry 12, Table 2). Another two new coupling partners, namely, 4-bromobenzotrifluoride (**1i**) and 1-iodo-3-nitrobenzene (**1j**), also furnished the corresponding unsymmetrical biaryls in 76% and 95% yields (entries 13 and 14, Table 2) when combined with 4-chlorophenylboronic acid (**2c**). The wide range of functional group tolerance of the present catalyst further motivated us to broaden the feasibility of GO-PdNPs toward the coupling of heteroaryl halides. 3-Bromopyridine (**1k**) was coupled with phenylboronic acid (**2a**) under ^{i}PrOH-K_2CO_3 combination, and 3-phenylpyridine (**3ka**) was obtained in quantitative yield (entry 1, Table 3). Further substrate scope was examined under identical conditions when 5-bromopyridin-2-amine (**1l**) and 3-bromoquinoline (**1m**) successfully furnished respective coupled products with phenylboronic acid (**2a**) in 86% and 99% yields (entries 2−3, Table 3). Again, 2-phenylthiophene was yielded quantitatively when 2-iodothiophene (**1n**) was allowed to couple with phenylboronic acid (entry 4, Table 3). A variety of substituted phenylboronic acids having acetyl (−C(O)Me), chloro (−Cl), methoxy (−OMe), trifluoromethyl (−CF_3), aldehyde (−CHO), and nitro (−NO_2) functional groups were then subjected to couple with 3-bromopyridine (entries 5−10, Table 3). The good to quantitative yields (58% to 99%) of these products indicate the versatility of the catalyst in Suzuki−Miyaura coupling. The successful syntheses of different heterobiaryls has been carried out using ^{i}PrOH-K_2CO_3 combination where the most utilized heteroaryl halide is 3-bromopyridine since the pyridine nucleus resides as an important scaffold in many pharmaceutically significant heterocyclic compounds.[47] Further, to compare the catalytic activity of the present PdNPs catalyst with that of conventional homogeneous catalyst $Pd(OAc)_2$, we performed catalytic experiments under identical palladium loading conditions. Three control experiments were carried out with $Pd(OAc)_2$ as a catalyst to prepare **3aa**, **3qc**, and **3la**, and the result points to the superior catalytic activity of GO-PdNPs as compared to homogeneous $Pd(OAc)_2$ (Supporting Information, Table S6).

With the convenient access to a variety of biaryls and heterobiaryls in good to quantitative yields, the catalytic activity

dx.doi.org/10.1021/cs400468h | *ACS Catal.* 2013, 3, 2776−2789

Table 2. Scope of the Suzuki–Miyaura Coupling Reaction Catalyzed by GO-PdNPs[a]

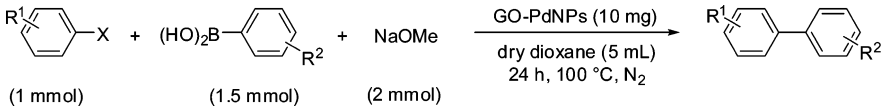

Entry	Aryl halide, **1**	Boronic acid, **2**	Biaryl, **3**	Yield (%) [b]
1	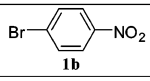 **1b**	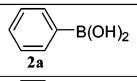 **2a**	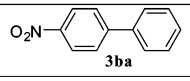 **3ba**	94
2	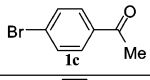 **1c**	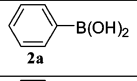 **2a**	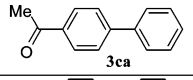 **3ca**	97
3	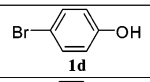 **1d**	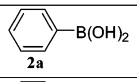 **2a**	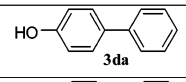 **3da**	98
4	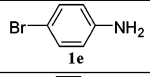 **1e**	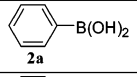 **2a**	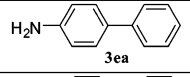 **3ea**	92
5	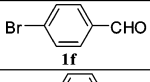 **1f**	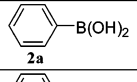 **2a**	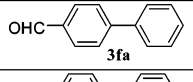 **3fa**	31
6	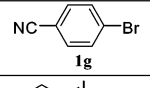 **1g**	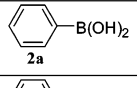 **2a**	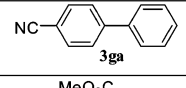 **3ga**	99
7	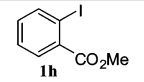 **1h**	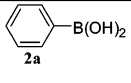 **2a**	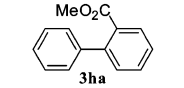 **3ha**	98
8	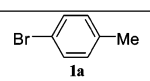 **1a**	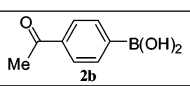 **2b**	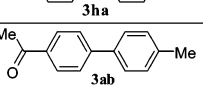 **3ab**	38
9	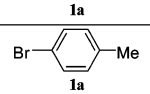 **1a**	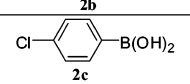 **2c**	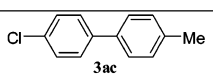 **3ac**	78
10	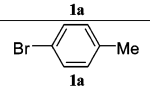 **1a**	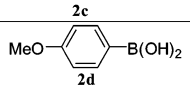 **2d**	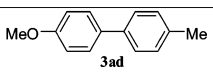 **3ad**	41
11	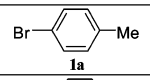 **1a**	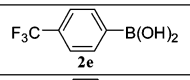 **2e**	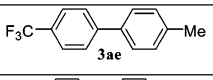 **3ae**	71
12	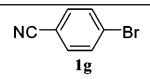 **1g**	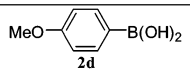 **2d**	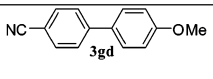 **3gd**	85
13	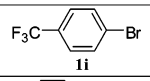 **1i**	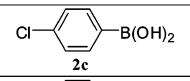 **2c**	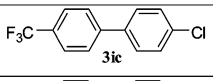 **3ic**	76
14	**1j**	**2c**	**3jc**	95

[a]Reaction conditions: GO-PdNPs (10 mg), aryl halide (1 mmol), boronic acid (2 mmol), and sodium methoxide (2 mmol) were reacted in 5 mL of dry dioxane in a 50 mL Schlenk flask under a N_2 atmosphere. [b]Yields were calculated after isolation of the pure biaryls through short column chromatography using silica gel (100–200 mesh).

of GO-PdNPs has been further examined toward the synthesis of core intermediates of two top selling drug molecules, namely an agricultural fungicide, boscalid,[48] and an angiotensin II receptor antagonist, telmisartan.[49] Also, the catalyst was tested to synthesize the core constituent of a selective PPARγ modulator, GSK376501A. Encouraged by the initial success of the Suzuki–Miyaura coupling reaction for a wide variety of substrates containing a variety of functional groups (Tables 2 and 3), herein, we report the quantitative synthesis of core intermediates of two top selling molecules, namely boscalid and telmisartan, as well as a selective PPARγ modulator, GSK376501A (Table 4). The boscalid nucleus has been synthesized under dioxane–NaOMe combination (entry 1, Table 4), while the synthesis of nuclei for telmisartan and GSK376501A has been accomplished under ^{i}the PrOH-K_2CO_3 recipe (entries 2 and 3, Table 4). The existing literature in this area mostly exploits phosphine-ligand-based palladium complexes for the syntheses of 4′-chloro-2-nitro-biphenyl (boscalid nucleus),[5,50] 2′-(4,4- dimethyl-4,5-dihydrooxazol-2-yl)biphenyl-4-carbaldehyde (telmisartan nucleus),[4] and ethyl 3-(4-*tert*-butylphenyl)-1*H*-indole-2-carboxylate (GSK376501A nucleus).[51] In this context, Kappe and Glasnov had shown the utilization of a flow reactor for continuous synthesis of boscalid where the Suzuki–Miyaura reaction was catalyzed by $[Pd(PPh_3)_4]$ under microwave irradiation.[5] Felpin et al. employed palladium on charcoal as a catalyst, resulting in 95% yield of the boscalid nucleus.[52] Pd/Cu cocatalyzed decarboxylative coupling of arylcarboxylic acids has also been established as an alternative approach for the synthesis of the boscalid nucleus by Gooßen and co-workers.[2] However, the existing scientific era lacks a potential heterogeneous catalyst which would be environmentally benign and economically attractive from the point of reusability.

dx.doi.org/10.1021/cs400468h | *ACS Catal.* 2013, 3, 2776–2789

Table 3. Synthesis of Heterobiaryls Catalyzed by GO-PdNPs[a]

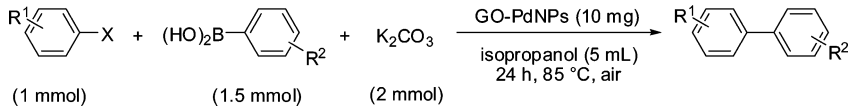

Entry	Aryl halide, **1**	Boronic acid, **2**	Biaryl, **3**	Yield (%)[b]
1	 **1k**	 **2a**	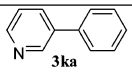 **3ka**	87
2	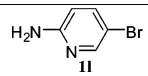 **1l**	 **2a**	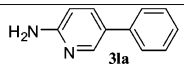 **3la**	86
3	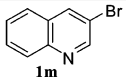 **1m**	 **2a**	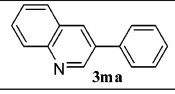 **3ma**	99
4	 **1n**	 **2a**	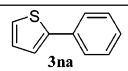 **3na**	98
5	 **1k**	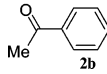 **2b**	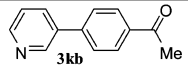 **3kb**	99
6	 **1k**	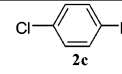 **2c**	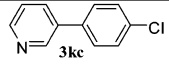 **3kc**	94
7	 **1k**	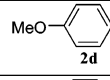 **2d**	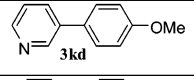 **3kd**	99
8	 **1k**	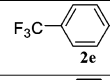 **2e**	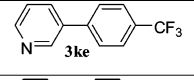 **3ke**	91
9	 **1k**	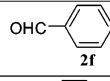 **2f**	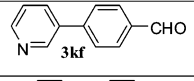 **3kf**	85
10	 **1k**	 **2g**	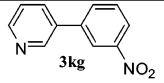 **3kg**	58

[a]Reaction conditions: GO-PdNPs (10 mg), aryl halide (1 mmol), boronic acid (2 mmol), and potassium carbonate (2 mmol) were reacted in 5 mL of isopropanol in a 50 mL round-bottom flask under air. [b]Yields were calculated after isolation of the pure biaryls through short column chromatography using silica gel (100−200 mesh).

Table 4. Synthesis of Pharmaceutically Active Intermediate Molecules *via* Suzuki−Miyaura Coupling Reaction

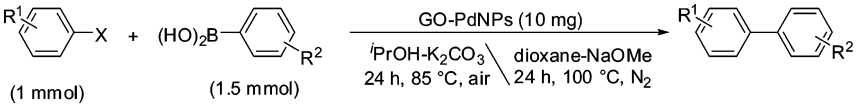

Entry	Aryl halide, **1**	Boronic acid, **2**	Biaryl, **3**	Yield (%)[a]
1[b]	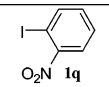 **1q**	 **2c**	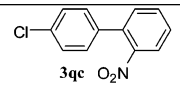 **3qc**	99
2[c]	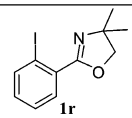 **1r**	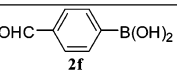 **2f**	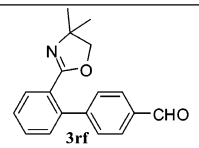 **3rf**	98
3[c]	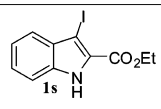 **1s**	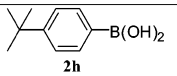 **2h**	**3sh**	89

[a]Yields were calculated after isolating the product through short column chromatography using silica gel (100−200 mesh). [b]GO-PdNPs (10 mg) was employed under dioxane−NaOMe combination. [c]GO-PdNPs (10 mg) was employed under ^{i}PrOH−K_2CO_3 combination.

An immense efficacy to recycle the catalyst for consecutive use is the finest part of any heterogeneous catalyst where the importance of the support reclines. The synthesis of core biaryls for boscalid and telmisartan in a recyclable manner has been taken as the choice to assess the recycling aptitude of the present catalyst GO-PdNPs. The recycling experiments were carried out after the isolation of the solid catalyst through membrane filtration techniques followed by a fresh batch of reactions with

dx.doi.org/10.1021/cs400468h | ACS Catal. 2013, 3, 2776−2789

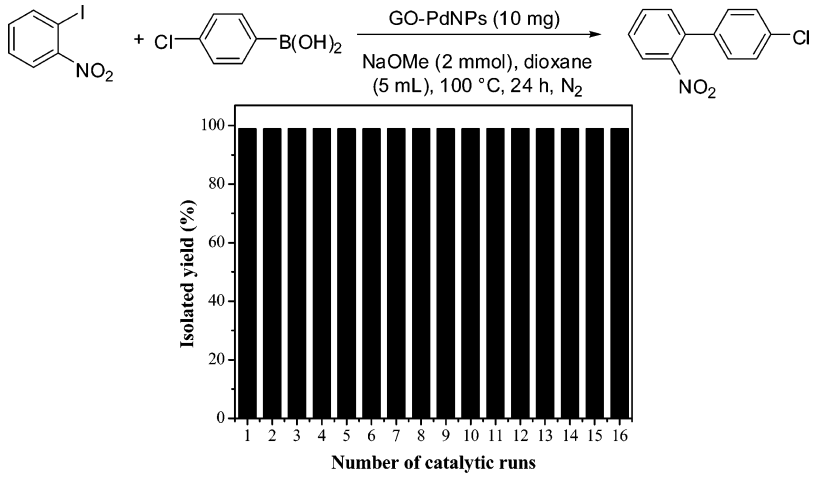

Figure 5. Recyclability chart of the catalytic reaction leading to the boscalid nucleus for successive 16 cycles.

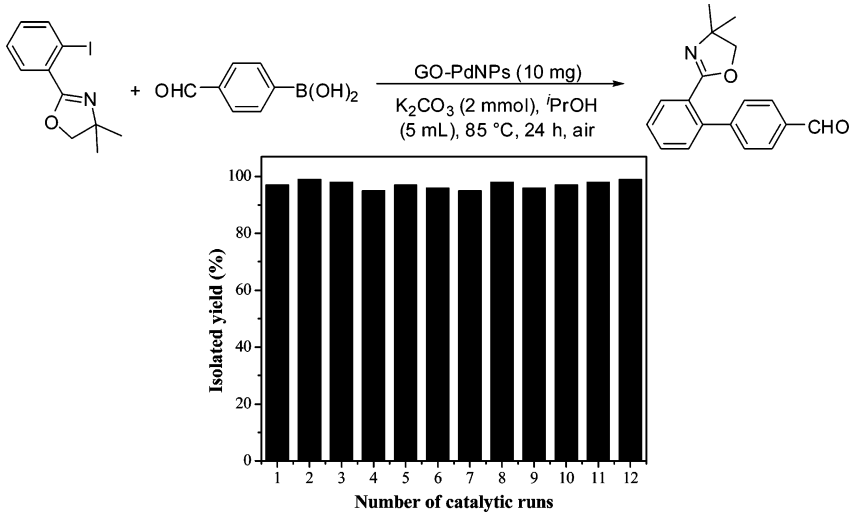

Figure 6. Recyclability chart of the catalytic reaction leading to the telmisartan nucleus for successive 12 cycles.

the recovered catalyst under identical reaction conditions. The recycling experiments for boscalid and telmisartan nuclei have been performed under dioxane-NaOMe and ^{i}PrOH-K_2CO_3 combinations, respectively. The results establish that GO-PdNPs remains equally active for 16 and 12 catalytic cycles for the synthesis of boscalid (Figure 5) and telmisartan nuclei (Figure 6), respectively, without any decay of the catalytic activity during the consecutive cycles. This recycling outcome of the present catalyst clearly points out the robust and sustained nature of the nanocatalyst. Further, we performed a control catalytic experiment using a physical mixture of GO and $Pd(OAc)_2$ for the synthesis of the boscalid nucleus under identical reaction condition (dioxane-NaOMe combination), adopted with the isolated GO-PdNPs. It shows that the first catalytic cycle leads to a much lower yield (34%) of the desired product as compared to the GO-PdNPs catalyst, and the recyclability experiment leads to no conversion in the second cycle (see Supporting Information, Scheme S1). This indicates that the isolation and prior preparation of the catalyst is important during which the palladium particles are gripped over the GO surface to ensure sustained recyclability.

We further took advantage of the catalytic activity in redesigning the existing synthetic route to the boscalid molecule in a more cost-effective two-step one-pot synthetic process where the most challenging part lies in the Suzuki−Miyaura coupling step between a haloaryl amine and corresponding boronic acid. The success of this particular step avoids the use of a hazardous hydrogenation step in the usual boscalid synthesis[5] involving a Suzuki−Miyaura coupling reaction followed by hydrogenation (Scheme 1). In the present study, the one-pot synthesis of boscalid was accomplished by subsequent addition of 2-nicotinyl chloride after the Suzuki−Miyaura process, resulting in 67% yield of boscalid. Notably, this particular Suzuki−Miyaura coupling step between the haloaryl amine and corresponding boronic acid has also been recycled with GO-PdNPs as catalyst, for six consecutive cycles with a quantitative yield of 4′-chlorobiphenyl-2-amine (Supporting Information, Figure S11). This recycling result again reflects the robustness of the catalyst.

From the HR-TEM studies after 16th and 12th catalytic cycles, during the course of the syntheses of boscalid and telmisartan nuclei, respectively, it was observed that the palladium particles maintain their nanodimension despite the harsh catalytic reaction conditions (Figure 7). However, from Figure 7, it is noticeable that migration and aggregation of palladium nanoparticles have taken place, forming bigger clusters during the recyclability process. There are few observable distinguished nanoparticles with size ranges between 6 and 22 nm (see Supporting Information, Figure S12).

dx.doi.org/10.1021/cs400468h | ACS Catal. 2013, 3, 2776−2789

Scheme 1. Cost-Effective Two-Step One-Pot Synthesis of Boscalid Accomplished Using GO-PdNPs As Catalyst Which Avoids the Hazardous Hydrogenation Step, Usually Involved in Boscalid Synthesis

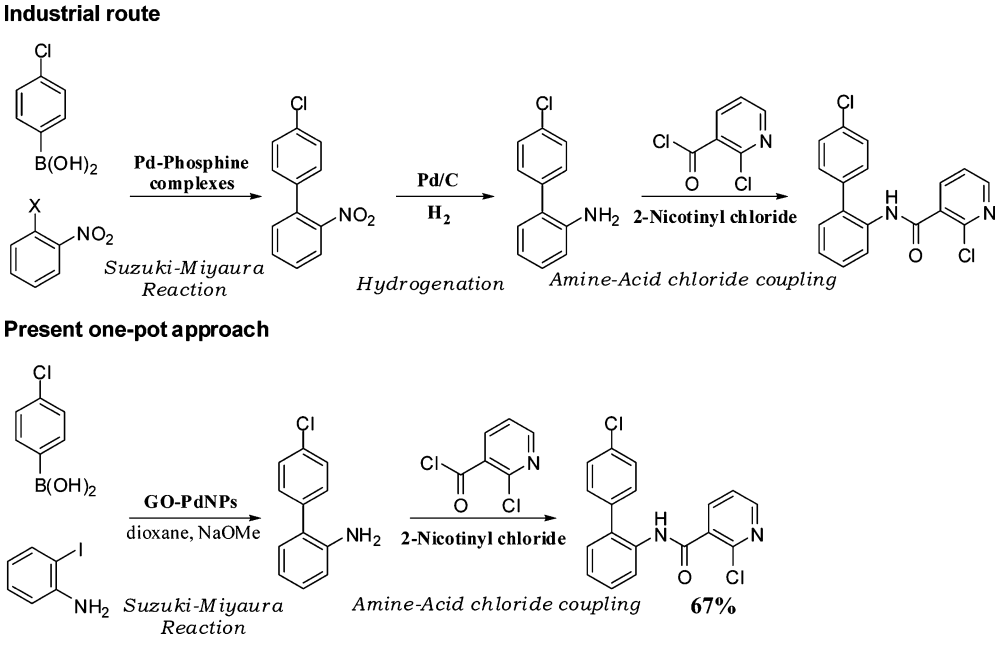

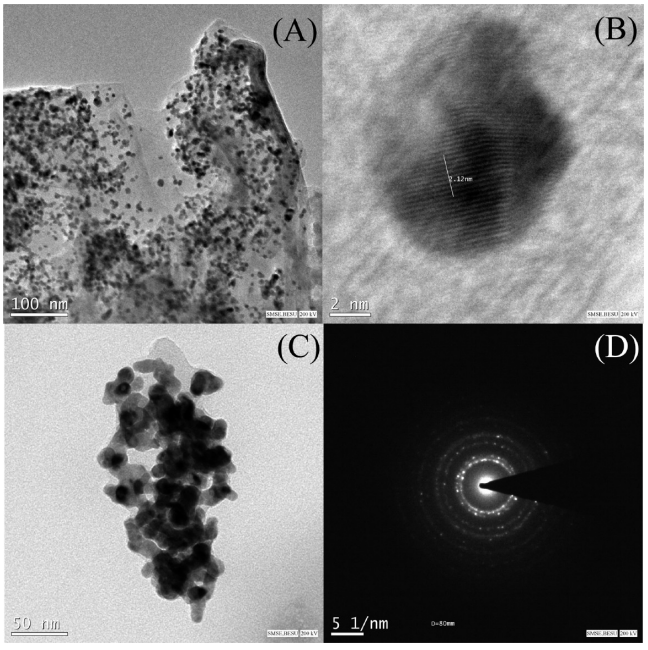

Figure 7. (A) TEM image of the catalyst after the 16th cycle of boscalid-nucleus synthesis from a very dilute ethanolic dispersion and (B) HR-TEM image of the same revealing the lattice fringe of PdNPs. (C) TEM image of the catalyst after the 12th cycle of telmisartan-nucleus synthesis from a very dilute ethanolic dispersion and (D) selected area electron diffraction pattern of Figure 7C.

The interplanar distance of 0.212 nm closely relates to that of an fcc lattice for palladium(0), confirming the survival of metallic nanopalladium clusters even after the 16th cycle of the boscalid-nucleus' synthesis (Figure 7B). The ICP-AES studies also detected no palladium contamination in two filtrates after the first catalytic run of each recyclability experiment, leading to the core moieties of boscalid and telmisartan (see Supporting Information, Table S5). The high competence of the present GO-PdNPs catalyst for its diverse functional group tolerance under Suzuki−Miyaura coupling reaction conditions and more importantly its nondecaying recycling efficiency for the preparation of top selling biaryl cores made us curious for further investigation on GO-PdNPs to understand the source of its sustained catalytic activity. To shed light on this aspect, we took help from IR, Raman, NMR spectroscopy, XPS, and a DFT modeling study.

The IR spectroscopic analysis was utilized to understand the interaction between Pd nanoparticles and different functionalities present in GO (Figure 8).[43,53,54] Notable frequency shifts

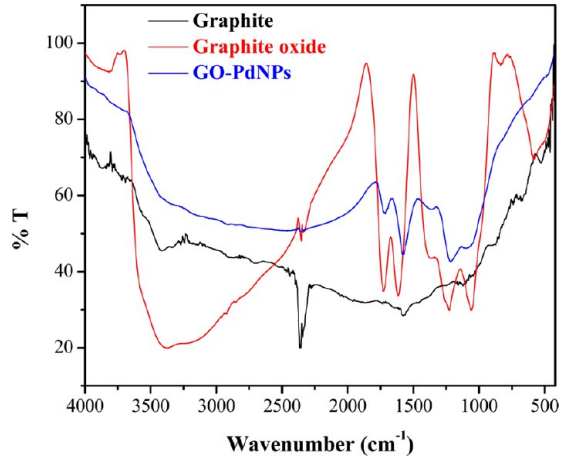

Figure 8. FT-IR spectra of graphite (black colored line), graphite oxide (red colored line), and GO-PdNPs (blue colored line).

($\Delta\nu$ = IR frequency observed in GO-PdNPs sample—IR frequency observed in GO) have been observed in the characteristic IR peaks of each functional group, which are as follows: (i) $\Delta\nu$ for C═O stretching vibrations = −16 cm^{-1}; (ii) $\Delta\nu$ for the skeletal vibrations of unoxidized graphitic regions comprising the sp^2 carbon network = −41 cm^{-1}; (iii) $\Delta\nu$ for the

dx.doi.org/10.1021/cs400468h | ACS Catal. 2013, 3, 2776−2789

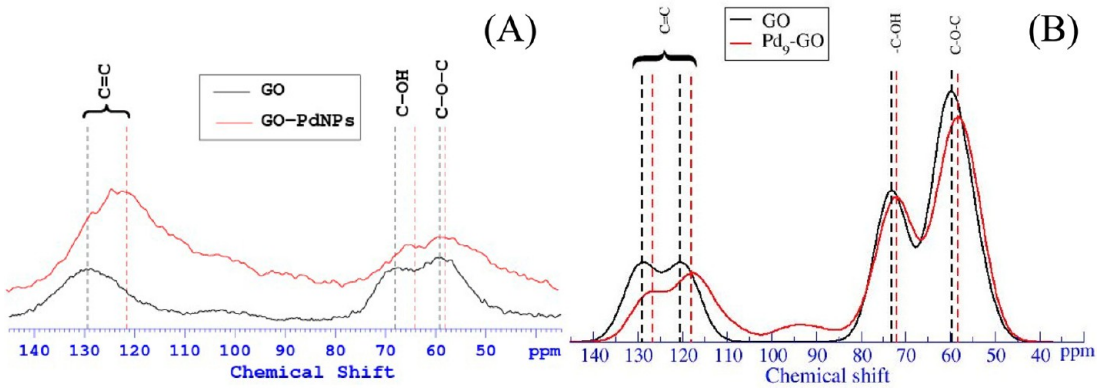

Figure 9. (A) Experimental solid-state ^{13}C MAS NMR spectra of graphite oxide (black colored line) and GO-PdNPs (blue colored line; full spectrum is presented in Supporting Information; Figure S13). (B) Simulated solid-state ^{13}C MAS NMR spectra of graphite oxide (black colored line) and GO-PdNPs (blue colored line).

bending frequency of tertiary alcoholic groups = −09 cm^{-1}; (iv) $\Delta\nu$ for the epoxy asymmetric stretching frequency = −13 cm^{-1}; and (v) $\Delta\nu$ for the epoxy C−O stretching frequency = +39 cm^{-1} (Supporting Information, Table S2). These IR spectroscopic shifts observed in the GO-PdNPs sample in comparison to the GO sample reflect a strong interaction between the functionalities present in GO with the palladium nanoparticles. Further, this fact is also supported by the ^{13}C solid state NMR spectroscopy. The incorporation of PdNPs onto GO commenced a shielding effect in diverse carbon environments when the materials were inspected through solid state ^{13}C NMR measurement with magic-angle spinning.[10,11] The major peaks at 59.6, 69.4, 130.5, and 194.8 ppm could be attributed to ^{13}C resonances of epoxy linkages, carbon atoms attached to hydroxyl groups, unoxidized sp^2 carbon network, and carbonyl moieties, respectively, in GO as studied by Lerf et al.[10] as well as by Ruoff and co-workers (Figure 9A; Supporting Information, Figure S13A).[11] After PdNPs' decoration, the ^{13}C resonances associated with different functional groups experienced a shielding effect having $\Delta\delta$ ($\Delta\delta$ = ^{13}C resonance of GO-PdNPs − ^{13}C resonance of GO) equal to −1.39, −4.19, −6.99, and −3.73 ppm values for epoxy linkages, carbon atoms attached to hydroxyl groups, unoxidized sp^2 carbon network, and carbonyl moieties, respectively (Figure 9A; Supporting Information Figure S13B and Table S3). This experimental observation was also further supported by our NMR simulation study on GO and GO-PdNPs. The structural models used for the calculation of the NMR spectra of GO and Pd_9-GO are shown in Figure 10A and B.[55] Similar to the experimental spectra, an overall shift of the NMR peaks toward lower ppm values was observed when Pd_9 binds to the GO. The C−O−C, C−OH, and sp^2 carbon peaks undergo shielding by −1.43, −1.05, −2.51, and −2.27 ppm, respectively (Figure 9B and Supporting Information, Table S4). The discrepancy in the absolute chemical shift values from the experimental study to the theoretical model can be attributed to the fact that PdNPs in the experiment are much bigger than the Pd cluster (Pd_9) considered in the present calculation and also the approximations used in the calculations. Nevertheless, the negative shift in both experimental and simulated spectra suggests that the binding interaction of palladium with different functionalities present in the graphite oxide results in a shielding effect in all of the ^{13}C resonances. The involvement of a π-network in the interaction has also been observed through the increment in I_D/I_G value (by 0.044) from GO to GO-PdNPs when the materials were subjected through resonance Raman spectroscopic analysis (Supporting Information, Figure S6).

In order to understand the interactions between the GO and the Pd nanoparticles more closely, we resorted to first principles total energy calculations. Among the different configurations considered in the calculations, the lowest energy binding configuration of Pd_9 on the GO sheet is shown in Figure 10B. In order to measure the stability of the cluster on the GO surface, we computed the binding energy per atom ($E_b = \{E_{Pd_9/GO} - E_{GO} - nE_{Pd}\}/n$, where $E_{Pd_9/GO}$, E_{GO}, and E_{Pd} are the total energies of the n atom Pd cluster on GO, the clean GO, and a single Pd atom in the gas phase). Our calculations yield a binding energy of −2.36 eV/Pd atom, which is comparable to the binding energy (about −2.53 eV/atom) of a 13 atom Pd cluster on γ-Al_2O_3 surfaces.[56] The strength of interaction between GO and Pd_9 is given by the adsorption energy ($E_{ads} = E_{Pd_9/GO} - E_{GO} - nE_{Pd_9}$, E_{Pd_9} is the total energy of the Pd cluster in the gas phase). We find the adsorption energy of Pd_9 on GO to be −1.70 eV, which is about 2 eV weaker compared to the most stable Pd_{13} cluster on (100) γ-Al_2O_3 surfaces and is very similar to those on the (110) surfaces of γ-Al_2O_3.[56] Our results suggest that the adsorption process leads to a stabilization of the Pd nanoparticles because the binding energy of the Pd cluster is lower than that of the gas phase by about 0.19 eV/atom. GO can anchor the Pd nanoparticles through covalent bonds between Pd atoms of the cluster which are in contact with the GO sheet and the C and O atoms of GO (bonds between C and O with Pd^1, Pd^2, and Pd^3 as shown in Figure 10B).

The model reveals that the Pd^1 center is asymmetrically bound to two sp^2 hybridized C atoms with Pd−C bond lengths of 2.27 and 2.49 Å. The Pd^1 center is also bound to a third sp^2 hybridized C atom with a slightly higher bond length of 2.74 Å and an O atom of the −OH group with a Pd−O bond length of 2.64 Å. Pd^2 is bound to another O atom of the −OH group, having a Pd−O bond length of 2.34 Å (Figure 10B). The O atom of the epoxy group forms another bond with the third palladium Pd^3 (Pd−O bond length = 2.04 Å). This type of bonding interaction of palladium centers through different functionalities and sp^2 hybridized C atoms results in multiple anchoring sites to hold the palladium nanoclusters tight on its surface. This structural model supports that PdNPs are strongly attracted on the GO sheet owing to the existence of multicentered chemical interactions. Further, to understand the nature of the bonding interaction and the origin of the shielding effect observed in our

dx.doi.org/10.1021/cs400468h | ACS Catal. 2013, 3, 2776−2789

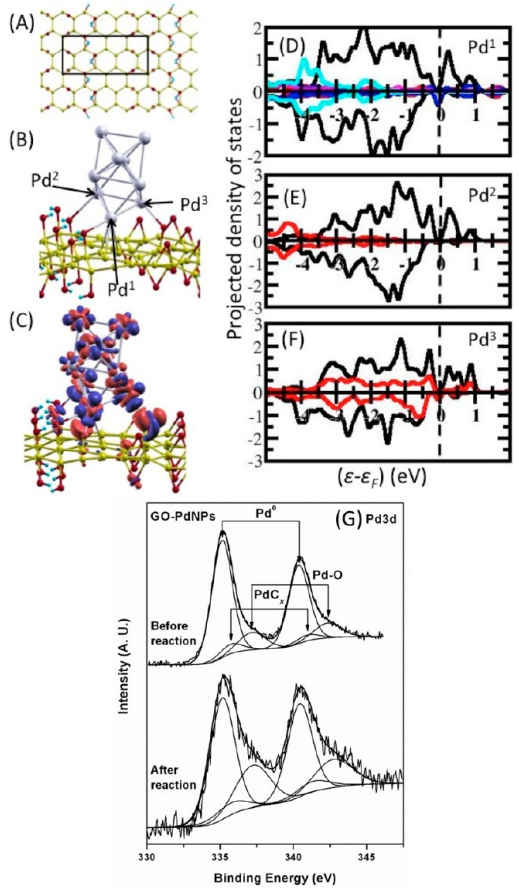

Figure 10. (A) The model GO sheet containing the epoxy, hydroxyl groups, and sp^2 hybridized C atoms. (B) Lowest energy binding configuration of Pd_9 on GO. (C) Isosurface corresponding to charge transfer between GO and Pd_9. Red (blue) isosurfaces denote regions of charge accumulation (depletion) (D) DOS projected on the d orbitals of Pd^1 (black shaded region) and the p orbitals of the three C atoms (red shaded region, blue and green lines) and the O atom (cyan lines) which form bonds with Pd^1. The projected DOS denoted by the red region and the blue lines are magnified 3 times their actual value for clarity. (E) DOS projected on the d orbitals of Pd^2 (black line) and the p orbitals of the O atom of −OH (red shaded region). (F) DOS projected on the d orbitals of Pd^3 (black line) and the p orbitals of the O atom of −OH (red shaded region). The C, O, H, and Pd atoms are denoted by yellow, red, cyan, and gray spheres, respectively. (G) XPS of Pd 3d core level in GO−PdNPs sample revealing the Pd−C and Pd−O bonding interaction before and after the catalytic cycle (detailed XPS results are presented in the Supporting Information).

solid state NMR experiments, we calculated the charge transfer between Pd_9 and the GO sheet and the projected density of states (DOS). The charge transfer isosurface is shown in Figure 10C. The Pd cluster becomes positively charged with 0.94 electrons being transferred from Pd_9 (mainly from the three Pd atoms, which interact with the O and C atoms of GO) to GO. These electrons are primarily localized on the O and the C atoms interacting with the Pd cluster. This charge transfer results in shielding effect observed in the solid state ^{13}C NMR spectrum of the GO-PdNPs. Figure 10C also shows that the charge transfer is essentially due to the interaction of the d orbitals of the Pd cluster and the p orbitals of O and C in GO. This fact is further strengthened from the projected DOS plots shown in Figure 10D−F. In each of these, the total DOS is projected onto the d orbitals of Pd and the p orbitals of the C and the O atoms involved in bond formation between Pd_9 and GO. The projected DOS in the three figures show that there is a strong overlap of the d states (primarily d_{zx}, d_{yz}, and d_{z^2}) of Pd with the p states of the C (p_z) and O (p_x) atoms. This suggests that there is a strong chemical bonding interaction between PdNPs and the different functional groups present in GO. These strong interactions help in anchoring the PdNPs onto the GO sheet, resulting in its sustained catalytic behavior over a large number of catalytic cycles.

In addition to the theoretical calculation, we have performed a detailed X-ray photoelectron spectroscopic (XPS) measurement to gain more insight into such bonding interactions between the PdNPs with GO functionalities. The XPS of Pd 3d core level in as-prepared GO-PdNPs is shown in Figure 10G (top spectrum). The Pd 3d spectral envelope indicates that Pd in the as-prepared GO-PdNPs sample is present in various oxidation states. The Pd $3d_{5/2,3/2}$ peaks are resolved into three sets of spin−orbit doublets by fixing the spin−orbit separation of 5.2 eV and ratio of doublet intensities at 3:2. Accordingly, Pd $3d_{5/2,3/2}$ peaks observed at 335.1 and 340.3 eV are ascribed to Pd metal only,[57] whereas peaks at 335.8 and 341 eV are assigned for PdC*x* species present on the surface;[58] an interaction is also noted from our first principles total energy calculations (see above). Peaks observed at 337.2 and 342.4 eV in the deconvoluted spectrum correspond to Pd $3d_{5/2,3/2}$ peaks of oxidized Pd−O species.[59,60] The presence of Pd−O bonding in the GO-PdNPs sample is further confirmed from the O 1s spectrum of the GO-PdNPs sample displaying an intensity enhancement at 530.5 eV peak upon Pd decoration (Supporting Information, Figure S7D). Furthermore, the C 1s spectrum of GO-PdNPs supports the charge transfer from palladium to carbon through a bonding interaction (Supporting Information, Figure S7C). Comparing the relative intensities of different Pd component peaks in the deconvoluted spectrum, it is to be noted that around 81% of the total Pd is in a metallic state, whereas oxidized species are present nearly 19% in the GO-PdNPs. Thus, XPS analysis demonstrates that the GO-PdNPs sample contains mainly Pd metal with a significant amount of Pd−O and Pd−C bonded species, as indicated by theoretical calculation. Figure 10G also represents a comparison of the Pd 3d core level XPS spectra for the PdNPs sample before catalysis (shown in top of Figure 10G) and after catalysis (shown in bottom of Figure 10G). The after catalysis sample was prepared from the catalytic run leading to the synthesis of 4-methylbiphenyl under a dioxane-NaOMe combination. The Pd 3d core level spectrum of the sample after catalysis shows metallic Pd as well as Pd−O and Pd−C bonded species. Though there is a little increase in the oxidized Pd component in the after catalysis sample, nevertheless the majority of Pd is present in the metallic state (70%) after the first catalytic run, demonstrating the stability of the catalyst.

In summary, a straightforward approach by pyrolysis has been described to anchor PdNPs onto the GO sheet, avoiding the use of any external reducing agent. The catalytic prominence of GO-PdNPs toward the Suzuki−Miyaura coupling reaction was established by creating a library of biaryls with a wide variety of functional group tolerance. The catalytic approach showed that GO-PdNPs is very active catalyst for the quantitative synthesis of core constituents of two top selling drug molecules, boscalid and telmisartan, together with biologically active GSK376501A. The catalyst GO-PdNPs displayed sustained recyclability over 10 cycles for production of the core biaryls of boscalid and telmisartan. The sustained catalytic activity of the present catalyst was attributed to a strong multicentered bonding interaction

dx.doi.org/10.1021/cs400468h | *ACS Catal.* 2013, 3, 2776−2789

with palladium nanoclusters and different chemical anchoring points present on the GO surface, which holds the palladium nanoclusters from leaching during catalysis.

■ ASSOCIATED CONTENT

Supporting Information

Supporting Information file contains AFM, TEM, SEM, EDX images of GO-PdNPs. UV−vis−NIR spectral as well as resonance Raman study together with XPS of the precursor and catalytic materials. Recyclability chart of a boscalid intermediate, 4′-chlorobiphenyl-2-amine, has also been represented along with the solid state NMR interpretation of the catalytic and precursor materials. It also contains spectroscopic data of organic compounds along with ^{1}H and ^{13}C NMR spectra. This material is available free of charge via the Internet at http://pubs.acs.org.

■ AUTHOR INFORMATION

Corresponding Author

*E-mail: swadhin.mandal@iiserkol.ac.in..

Notes

The authors declare no competing financial interest.

■ ACKNOWLEDGMENTS

This work is dedicated to Dr. R. A. Mashelkar on the occasion of his 70th birthday. S.K.M. thanks SERB (DST, No. SR/S1/IC-25/2012), India for financial support. S.S. thanks CSIR, India for a research fellowship. The authors gratefully acknowledge Mr. Arnab Maity and Mr. Abhisek Basu for collecting AFM images and Raman data, respectively. We are thankful to Dr. Suhrit Ghosh's group at IACS, India for SEM analysis. The authors thank the instrumental facilities of IISER-Kolkata. The authors gratefully acknowledge Mr. Susanta Bhunia and Mr. Arjyabaran Sinha at IACS, India for the ICP-AES study. P.G. acknowledges IISER-Pune and Centre for Development of Advanced Scientific Computing, Pune, India for providing the HPC facility and financial support from DST-Nano Mission Project No: SR/NM/NS-15/2011. P.G. also wants to thank Dr. Anirban Hazra, IISER Pune, and Dr. Varadharajan Srinivasan, IISER Bhopal, India for allowing him to access their computational facilities, without which it would not have been possible to calculate the O 1s core level spectra. The authors thank the anonymous reviewers for their valuable suggestions.

■ REFERENCES

(1) Bringmann, G.; Gulder, T.; Gulder, T. A. M.; Breuning, M. *Chem. Rev.* **2011**, *111*, 563−639.
(2) Gooßen, L. J.; Deng, G.; Levy, L. M. *Science* **2006**, *313*, 662−664.
(3) Ghosh, S.; Kumar, A. S.; Mehta, G. N. *Beilstein J. Org. Chem.* **2010**, *6* (No. 27), 1−4, DOI: 10.3762/bjoc.6.27.
(4) Kumar, A. S.; Ghosh, S.; Mehta, G. N. *Beilstein J. Org. Chem.* **2010**, *6* (No. 25), 1−5, DOI: 10.3762/bjoc.6.25.
(5) Glasnov, T. N.; Kappe, C. O. *Adv. Synth. Catal.* **2010**, *352*, 3089−3097.
(6) Bullock, K. M.; Burton, D.; Corona, J.; Diederich, A.; Glover, B.; Harvey, K.; Mitchell, M. B.; Trone, M. D.; Yule, R.; Zhang, Y.; Toczko, J. F. *Org. Process Res. Dev.* **2009**, *13*, 303−309.
(7) Torborg, C.; Beller, M. *Adv. Synth. Catal.* **2009**, *351*, 3027−3043.
(8) Butters, M.; Catterick, D.; Craig, A.; Curzons, A.; Dale, D.; Gillmore, A.; Green, S. P.; Marziano, I.; Sherlock, J.-P.; White, W. *Chem. Rev.* **2006**, *106*, 3002−3027.
(9) Gruttadauria, M.; Liotta, L. F.; Salvo, A. M. P.; Giacalone, F.; Parola, V. L.; Aprile, C.; Noto, R. *Adv. Synth. Catal.* **2011**, *353*, 2119−2130.
(10) Lerf, A.; He, H.; Forster, M.; Klinowski, J. *J. Phys. Chem. B* **1998**, *102*, 4477−4482.
(11) Cai, W.; Piner, R. D.; Stadermann, F. J.; Park, S.; Shaibat, M. A.; Ishii, Y.; Yang, D.; Velamakanni, A.; An, S. J.; Stoller, M.; An, J.; Chen, D.; Ruoff, R. S. *Science* **2008**, *321*, 1815−1817.
(12) Rourke, J. P.; Pandey, P. A.; Moore, J. J.; Bates, M.; Kinloch, I. A.; Young, R. J.; Wilson, N. R. *Angew. Chem., Int. Ed.* **2011**, *50*, 3173−3177.
(13) Tang, Z.; Shen, S.; Zhuang, J.; Wang, X. *Angew. Chem., Int. Ed.* **2010**, *49*, 4603−4607.
(14) Cheng, J.; Zhang, G.; Du, J.; Tang, L.; Xu, J.; Li, J. *J. Mater. Chem.* **2011**, *21*, 3485−3494.
(15) Scheuermann, G. M.; Rumi, L.; Steurer, P.; Bannwarth, W.; Mülhaupt, R. *J. Am. Chem. Soc.* **2009**, *131*, 8262−8270.
(16) Moussa, S.; Siamaki, A. R.; Gupton, B. F.; El-Shall, M. S. *ACS Catal.* **2012**, *2*, 145−154.
(17) Nishina, Y.; Miyata, J.; Kawai, R.; Gotoh, K. *RSC Adv.* **2012**, *2*, 9380−9382.
(18) Mastalir, Á.; Király, Z.; Benkő, M.; Dékány, I. *Catal. Lett.* **2008**, *124*, 34−38.
(19) Gotoh, K.; Kawabata, K.; Fujii, E.; Morishige, K.; Kinumoto, T.; Miyazaki, Y.; Ishida, H. *Carbon* **2009**, *47*, 2112−2142.
(20) He, H.; Gao, C. *Molecules* **2010**, *15*, 4679−4694.
(21) Chen, X.; Wu, G.; Chen, J.; Chen, X.; Xie, Z.; Wang, X. *J. Am. Chem. Soc.* **2011**, *133*, 3693−3695.
(22) Chandra, S.; Bag, S.; Das, P.; Bhattacharya, D.; Pramanik, P. *Chem. Phys. Lett.* **2012**, *519*−*520*, 59−63.
(23) Li, W.; Geng, X.; Guo, Y.; Rong, J.; Gong, Y.; Wu, L.; Zhang, X.; Li, P.; Xu, J.; Cheng, G.; Sun, M.; Liu, L. *ACS Nano* **2011**, *9*, 6955−6961.
(24) Kumar, R.; Varandani, D.; Mehta, B. R.; Singh, V. N.; Wen, Z.; Feng, X.; Müllen, K. *Nanotechnology* **2011**, *22*, 275719.
(25) Ioni, Y. V.; Lyubimov, S. E.; Davankov, V. A.; Gubin, S. P. *Russ. J. Inorg. Chem.* **2013**, *58*, 392−394.
(26) Siamaki, A. R.; Khder, A. E. R. S.; Abdelsayed, V.; El-Shall, M. S.; Gupton, B. F. *J. Catal.* **2011**, *279*, 1−11.
(27) Chen, H.; Li, Y.; Zhang, F.; Zhang, G.; Fan, X. *J. Mater. Chem.* **2011**, *21*, 17658−17661.
(28) Giannozzi, P.; Baroni, S.; Bonini, N.; Calandra, M.; Car, R.; Cavazzoni, C.; Ceresoli, D.; Chiarotti, G. L.; Cococcioni, M.; Dabo, I.; Corso, A. D.; de Gironcoli, S.; Fabris, S.; Fratesi, G.; Gebauer, R.; Gerstmann, U.; Gougoussis, C.; Kokalj, A.; Lazzeri, M.; Martin-Samos, L.; Marzari, N.; Mauri, F.; Mazzarello, R.; Paolini, S.; Pasquarello, A.; Paulatto, L.; Sbraccia, C.; Scandolo, S.; Sclauzero, G.; Seitsonen, A. P.; Smogunov, A.; Umari, P.; Wentzcovitch, R. M. *J. Phys.: Condens. Matter* **2009**, *21*, 395502.
(29) Vanderbilt, D. *Phys. Rev. B* **1990**, *41*, 7892−7895.
(30) Perdew, J. P.; Burke, K.; Ernzerhof, M. *Phys. Rev. Lett.* **1996**, *77*, 3865−3868.
(31) Monkhorst, H. J.; Pack, J. D. *Phys. Rev. B* **1976**, *13*, 5188−5192.
(32) Marzari, N.; Vanderbilt, D.; DeVita, A.; Payne, M. C. *Phys. Rev. Lett.* **1999**, *82*, 3296−3299.
(33) Zanti, G.; Peeters, D. *Eur. J. Inorg. Chem.* **2009**, 3904−3911.
(34) Yan, J.-A.; Chou, M. Y. *Phys. Rev. B* **2010**, *82*, 125403.
(35) Wang, L.-L.; Johnson, D. D. *J. Am. Chem. Soc.* **2007**, *129*, 3658−3664.
(36) Ravon, U.; Chaplais, G.; Chizallet, C.; Seyyedi, B.; Bonino, F.; Bordiga, S.; Bats, N.; Farrusseng, D. *ChemCatChem.* **2010**, *2*, 1235−1238.
(37) Pickard, C. J.; Mauri, F. *Phys. Rev. B* **2001**, *63*, 245101.
(38) Hummers, W. S., Jr.; Offeman, R. E. *J. Am. Chem. Soc.* **1958**, *80*, 1339−1339.
(39) Liao, K.-H.; Mittal, A.; Bose, S.; Leighton, C.; Khoyan, K. A.; Macosko, C. W. *ACS Nano* **2011**, *5*, 1253−1258.
(40) Niedermann, K.; Welch, J. M.; Koller, R.; Cvengroš, J.; Santschi, N.; Battaglia, P.; Togni, A. *Tetrahedron* **2010**, *66*, 5753−5761.
(41) Santra, S.; Dhara, K.; Ranjan, P.; Bera, P.; Dash, J.; Mandal, S. K. *Green Chem.* **2011**, *13*, 3238−3247.
(42) Santra, S.; Ranjan, P.; Bera, P.; Ghosh, P.; Mandal, S. K. *RSC Adv.* **2012**, *2*, 7523−7533.

(43) Ganesan, M.; Freemantle, R. G.; Obare, S. O. *Chem. Mater.* **2007**, *19*, 3464−3471.
(44) Yeh, T.-F.; Syu, J.-M.; Cheng, C.; Chang, T.-H.; Teng, H. *Adv. Funct. Mater.* **2010**, *20*, 2255−2262.
(45) Yang, S.; Shen, C.; Lu, X.; Tong, H.; Zhu, J.; Zhang, X.; Gao, H.-J. *Electrochim. Acta* **2012**, *62*, 242−249.
(46) Shen, J.; Hu, Y.; Shi, M.; Li, N.; Ma, H.; Ye, M. *J. Phys. Chem. C* **2010**, *114*, 1498−1503.
(47) Carey, J. S.; Laffan, D.; Thomson, C.; Williams, M. T. *Org. Biomol. Chem.* **2006**, *4*, 2337−2347.
(48) Matheron, M. E.; Porchas, M. *Plant Dis.* **2004**, *88*, 665−668.
(49) Sharpe, M.; Jarvis, B.; Goa, K. L. *Drugs* **2001**, *61*, 1501−1529.
(50) Spivey, A. C.; Tseng, C.-C.; Hannah, J. P.; Gripton, C. J. G.; de Fraine, P.; Parr, N. J.; Scicinski, J. J. *Chem. Commun.* **2007**, 2926−2928.
(51) Bullock, K. M.; Mitchell, M. B.; Toczko, J. F. *Org. Process Res. Dev.* **2008**, *12*, 896−899.
(52) Felpin, F.-X.; Fouquet, E.; Zakri, C. *Adv. Synth. Catal.* **2009**, *351*, 649−655.
(53) Jeong, H.-K.; Lee, Y. P.; Lahaye, R. J. W. E.; Park, M.-H.; An, K. H.; Kim, I. J.; Yang, C.-W.; Park, C. Y.; Ruoff, R. S.; Lee, Y. H. *J. Am. Chem. Soc.* **2008**, *130*, 1362−1366.
(54) Zhang, Y.; Pan, C. *J. Mater. Sci.* **2011**, *46*, 2622−2626.
(55) Yan, J.-A.; Xian, L.; Chou, M. Y. *Phys. Rev. Lett.* **2009**, *103*, 086802.
(56) Hu, C. H.; Chizallet, C.; Mager-Maury, C.; Corral-Valero, M.; Sautet, P.; Toulhoat, H.; Raybaud, P. *J. Catal.* **2010**, *274*, 99−110.
(57) Brun, M.; Berthet, A.; Bertolini, J. C. *J. Electron Spectrosc. Relat. Phenom.* **1999**, *104*, 55−60.
(58) Balmes, O.; Resta, A.; Wermeille, D.; Felici, R.; Messing, M. E.; Deppert, K.; Liu, Z.; Grass, M. E.; Bluhm, H.; van Rijn, R.; Frenken, J. W. M.; Westerström, R.; Blomberg, S.; Gustafson, J.; Andersen, J. N.; Lundgren, E. *Phys. Chem. Chem. Phys.* **2012**, *14*, 4796−4801.
(59) Kim, J. Y.; Park, K.; Bae, S. Y.; Kim, G. C.; Lee, S.; Choi, H. C. *J. Mater. Chem.* **2011**, *21*, 5999−6005.
(60) Wagner, C. D.; Riggs, W. M.; Davis, L. E.; Moulder, J. F. *Handbook of X-Ray Photoelectron Spectroscopy*; Muilenberg, G. E., Ed.; PerkinElmer: Eden Prairie, MN, 1979.